A promyelocytic leukaemia protein-thrombospondin 2 axis and the risk of relapse in neuroblastoma

Maria Dvorkina[a1], Valentina Nieddu[b,c,d,1], Shalini Chakelam[a,2], Annalisa Pezzolo[e,2], Sandra Cantilena[b,f], Ana Paula Leite[a], Olesya Chayka[b,f], Tarik Regad[a,g], Angela Pistorio[h], Angela Rita Sementa[i], Alex Virasami[f,j], Jack Barton[f,j], Ximena Montano[f,j], Tanguy Lechertier[k], Nicola Brindle[a], Daniel Morgenstern[f,j], Morgane Lebras[l], Alan Burns[f], Nigel Saunders[b], Kairbaan Hodivala-Dilke[k], Luigi Bagella[c,d], Hugues De The[l], John Anderson[f,j], Neil Sebire[f,j], Vito Pistoia[h], Arturo Sala[b,f,2] and Paolo Salomoni[a,2].

Affiliations:

[a]University College London Cancer Institute, Samantha Dickson Brain Cancer Unit, UCL, London, UK;

[b]Department of Life Sciences, Brunel University London, Uxbridge, UK;

[c]Department of Biomedical Sciences, and National Institute of Biostructures and Biosystems, University of Sassari, Sassari, Italy;

[d]Sbarro Institute for Cancer Research and Molecular Medicine, Center for Biotechnology, College of Science and Technology, Temple University, Philadelphia, USA

[e]Laboratorio di Oncologia, Istituto Giannina Gaslini, Genova, Italy;

[f]UCL Institute of Child Health, London, UK;

[g]Nottingham Trent University, Nottingham, UK;

[h]Laboratorio di Anatomia Patologica, Istituto Giannina Gaslini, Genova, Italy;

[i]Epidemiologia e Biostatistica, Istituto Giannina Gaslini, Genova, Italy;

[j]Great Ormond Street Hospital, London, UK;

[k]Barts Cancer Institute, Queen Mary University, London, UK;

[l]Institut Universitaire d'Hematologie, Sant-Louis Hospital, Paris-Diderot, France;

[1]Equal contribution (First author)

[2]Equal contribution (Second author)

[3]*Corresponding authors*: **Paolo Salomoni**, UCL Cancer Institute, Samantha Dickson Brain Cancer Unit, University College London WC1E 6DD, London UK; email: p.salomoni@ucl.ac.uk; or **Arturo Sala**, Department of Life Sciences, Brunel University London, UB8 3PH, Uxbridge UK; email: arturo.sala@brunel.ac.uk

Running title: A PML-I/thrombospondin-2 axis regulates angiogenesis

We do not have any conflict of interest to disclose

Translational relevance

Neuroblastoma is a childhood malignancy originating from the sympathetic nervous system that is prone to metastasize and relapse. PML is a tumour suppressor gene frequently deregulated in cancer, but its prognostic and functional significance in neuroblastoma is unknown. A fraction of localized neuroblastomas recur locally after surgery and can do so several times in spite of further treatments, eventually killing the patient. In this study we have established that PML-I is a negative regulator of angiogenesis via activation of thrombospondin-2 and its reduced or absent expression in localized neuroblastoma is an accurate marker of the risk of relapse. An important clinical implication of our study is that PML expression could be now used to identify patients with low-risk, localized tumors needing systemic treatments to avoid cancer recurrence.

Abstract

Purpose. Neuroblastoma is a childhood malignancy originating from the sympathetic nervous system with a complex biology, prone to metastasize and relapse. High-risk, metastatic cases are explained in part by amplification or mutation of oncogenes such as MYCN and ALK and loss of tumour suppressor genes in chromosome band 1p. However, it is fundamental to identify other pathways responsible for the large portion of neuroblastomas with no obvious molecular alterations.

Experimental design. Neuroblastoma cell lines were used for assessment of tumour growth *in vivo* and *in vitro*. Protein expression in tissues and cells was assessed using immunofluorescence and immunohistochemistry. The association of PML expression with neuroblastoma outcome and relapse was calculated using log-rank and Mann-Whitney tests, respectively. Gene expression was assessed using chip microarrays.

Results: PML is detected in the developing and adult sympathetic nervous system, whereas it is not expressed or low in metastatic neuroblastoma tumours. Reduced PML expression in patients with low-risk cancers - i.e. localized and negative for the MYCN protooncogene - is strongly associated with tumour recurrence. PML-I, but not PML-IV, isoform suppresses angiogenesis via upregulation of thrombospondin-2 (TSP-2), a key inhibitor of angiogenesis. Finally, PML-I and TSP-2 expression inversely correlates with tumour angiogenesis and recurrence in localized neuroblastomas.

Conclusions: Our work reveals a novel PML-I-TSP2 axis for regulation of angiogenesis and cancer relapse, which could be used to identify patients with low-risk, localized tumours that might benefit from chemotherapy.

Key words: paediatric oncology, PML, thrombospondin, neuroblastoma, MYCN

Introduction

The Promyelocytic Leukaemia protein (PML) is a growth/tumour suppressor inactivated in Acute Promyelocytic Leukaemia (APL) via the t(15;17) translocation. PML is expressed as multiple splice variants and is the essential component of a subnuclear structure called the PML nuclear body (PML-NB), which is disrupted in APL (1). PML has emerged as pleiotropic growth suppressor affecting multiple cellular pathways involved in tumourigenesis, in part via recruitment of nuclear factors to the PML-NBs, also required for activation of p53 (2-8). One of the main physiological roles of PML is its ability to regulate cell fate in stem/progenitor cells in multiple tissues (9). In the nervous system, we have shown that PML regulates neurogenesis and cortex development by modifying the Retinoblastoma (pRb) G1/S checkpoint (9, 10). Most growth and tumour suppressive activities of PML have been linked to the splice variant PML-IV (11), whereas little is known about the other more abundant variants, such as PML-I (12, 13). PML expression is lost in tumours of multiple histological origins, and its inactivation has been shown to promote tumour progression in APL, prostate and lung cancer (5, 14-16). In contrast, it may play an oncogenic role in chronic myeloid leukaemia and breast cancer (17, 18). PML role in tumours of the nervous system has not been investigated.

Neuroblastoma is the most common extra-cranial solid tumour in childhood and the most frequently diagnosed malignancy in infancy. It accounts for 8% of cancer cases in children and approximately 15% of all childhood cancer deaths, highlighting the aggressive nature of this tumour (19, 20). The tumour develops from neural crest-derived sympathoadrenal precursor cells (20). Neuroblastoma is characterized by a number of genetic aberrations; these include ploidy changes, gains of chromosome arm 17q, amplification of the proto-oncogene *MYCN,* activating mutations of ALK, and deletions of different genomic regions containing putative tumour suppressor genes in chromosome bands 11q23, 1p36 and 14q23-qter(19, 21-24). Neuroblastomas commonly arise from the medullary region of the adrenal gland (20, 25) and are classified into five stages (1-4 and 4S), according to the International Neuroblastoma Staging System (INSS) (26, 27). Low-risk patients (stages 1, 2 and 4S with a favourable histology) have a survival rate greater than 85% whereas the survival rate for high-risk neuroblastoma (stages 3,4 with unfavourable histology and MYCN amplification) is less than 50% in spite of multimodal therapy, reflecting the propensity of the tumour to relapse into a treatment resistant, fatal form of the disease (20, 27, 28). Recurrent neuroblastoma in patients initially classified as low-risk is uncommon, but can develop into an intractable cancer. It would

be very important to identify patients at risk of recurrence needing chemotherapy in addition to surgical removal of the localized tumour mass.

In this study, we show that PML expression inversely correlates with tumour relapse in localized neuroblastomas and is lost in aggressive forms of human and mouse neuroblastomas. The PML-I isoform, when overexpressed in neuroblastoma cells, does not affect proliferation or survival, but instead it suppresses angiogenesis *in vitro* and *in vivo*. Mechanistically, PML-I inhibits angiogenesis by upregulating Thrombospondin-2, a known angiogenesis suppressor. Finally, PML-I expression inversely correlates with tumour angiogenesis in primary tumour samples. Overall, these data implicate PML in isoform-specific regulation of neuroblastoma pathogenesis and suggest that it may serve as predictor of relapse in localized neuroblastoma.

Materials and Methods

Cell culture. IMR32, SH-EP, SK-N-SH, SK-N-AS, Kelly, NB69 and LAN-5 human neuroblastoma lines were a kind gift from Dr Louis Chesler's lab (Institute of Cancer Research, London, UK). SHSY5Y human neuroblastoma cell line was purchased from ATCC. The cells were cultured in DMEM- or RPMI-based media supplemented with 10% foetal calf serum, 2 mM L-glutamine, 100 mg/mL penicillin and 100 mg/mL streptomycin. Cell lines were sent to Public Health England or DDC Medical for authentication. The validation method used was Short Tandem Repeat (STR) assay. For *ex vivo* mouse neural crest trunk progenitor cultures, the neural tubes were dissected from e9.5 C57BL/6 mouse embryos, and the trunk section of the tube was placed on laminin/fibronectin-covered coverslip and left to attach in a drop of dissection medium (DMEM:F-12 medium 1:1 +5%FCS+100 mg/mL penicillin+100 mg/mL streptomycin). The explants were cultured for 24-48 hours in neural tube culture medium (DMEM/F12 1:1 supplemented with N2, B27 (both Invitrogen), bFGF 20ng/ml and EGF 20ng/ml. The coverslips with the neural tube explants and migrated progenitors were fixed in 4% PFA and used for immunostaining.

Cell proliferation assessment. Cells were plated in 12-well plates and cultured until fully confluent. During the culturing period, images were acquired at regular intervals using IncuCyte live-cell imaging system (Essen Biosciences) and processed using the IncuCyte software to calculate the growth rates.

Patients and Clinical Follow-up. A retrospective series of primary tumours from neuroblastoma (NB) patients (Table 1, Supplementary Tables 1 and 2) was collected at the Istituto Giannina Gaslini, Genova, Italy (January 2000 to December 2008) and Great Ormond Street Hospital (GOSH)/UCL Institute of Child Health (until 2013). All patients included in the Gaslini cohort received surgical treatment, and the only inclusion criterion was the availability of the complete clinical records. The study was approved by the respective Institutional Review Boards and informed consent was obtained from patients or their legal guardians at both institutions. Patients were classified according to the International Neuroblastoma Staging System classification (29). Event-Free Survival (EFS) was calculated from diagnosis to last follow-up or event (first occurrence of relapse, progression, or death).

Tumour Specimens. Formalin-fixed, paraffin-embedded tissue sections from NB tumours were studied. Each tumour area tested contained malignant cells, as assessed by histological examination. Quantification of immunofluorescence- or DAB-positive tumour cells was performed on serial tumour tissue sections, thus allowing quantification in tumour areas

selected by the pathologist. Tumour cells were distinguished in the samples using NB-specific marker NCAM (NB56). The adhesion molecule NCAM has been shown to be widely and brightly expressed on NB tumours (30). All tumours were evaluated at the time of diagnosis prior to any treatment other than surgery.

Immunostaining of cultured cells. For immunostaining of human or mouse cells in culture, cells were grown on poly-D-lysine coated coverslips and fixed with 4% PFA. Tissue sections or cells were permeabilised with 0.5% Triton-X100, subjected to antigen retrieval (tissue sections only), blocked using 10% normal goat serum/2.5%BSA/0.1% PBS-Tween and incubated with a primary antibody diluted in blocking solution overnight at 4°C, followed by incubation with a secondary antibody (AlexaFluor, Invitrogen) in blocking solution for 1 hour at room temperature, counterstained with Hoechst and mounted for microscopy.

Immunofluorescence analysis and quantifications of micro-vessel density in tissue samples. Mouse tissue samples were fixed in 4% PFA, dehydrated and embedded in paraffin or preserved by snap-freezing in liquid N_2. Tissue sections were cut and mounted on glass slides. Paraffin-embedded sections were deparaffinised and rehydrated. Frozen sections were fixed in 4% PFA or cold acetone (specific for CD31 staining). Standard histochemical protocol was used for haematoxylin and eosin staining. Indirect immunofluorescence was performed on formalin-fixed, paraffin embedded tissues from 30 primary NB tumours as previously described (31). Paraffin sections (4 µm thick) were processed by standard deparaffinisation with xylene and hydrated in a descending ethanol series to double-distilled water. Antigen retrieval on formalin-fixed tissue section was performed using Sodium-Citrate buffer (pH 6.0). Slides were incubated with primary antibodies overnight at 4°C. Secondary antibodies used were: goat anti-mouse IgG Alexa-488, goat anti-rabbit IgG Alexa-568 (diluted 1:200; Invitrogen, Germany), donkey anti-goat IgG-NL557 (diluted 1:200; R&D Systems, Inc, Europe). After washing, the slides were counterstained with 4',6'-diamidino-2- phenylindole (DAPI, Sigma-Aldrich, Milan, Italy) and cover-slipped. The proportion of immunofluorescence positive tumour cells counted was at least 100-1000 cells and reported in the percentage for the subsequent statistical analysis. The micro-vessel count (MVC) was assessed by anti-CD31 staining and examination of twenty microscopic fields (0.5 mm^2) per tumour. The most intense vascular areas (hotspots) were selected subjectively from each tumour section. The micro-vessels with a clearly defined lumen or well-defined linear vessel shape were taken into account for MVC.

Digital images were collected using a Nikon E-1000 fluorescence microscope (Nikon Instruments, Tokyo, Japan) equipped with appropriate filter sets and the Genikon imaging system software (Nikon Instruments).

Western blotting. Cells were lysed in Laemmli buffer supplemented with β-mercaptoethanol. The proteins were resolved on SDS-PAGE and transferred onto nitrocellulose or PVDF membranes. Membranes were incubated overnight with the primary antibodies followed by incubation with HRP-conjugated secondary antibodies (Amersham) and ECL substrate (Thermo Scientific™).

Angiogenesis assay. The angiogenesis assay was performed using the *in vitro* angiogenesis kit (Cellworks #ZHA4000). In brief, human umbilical vein endothelial cells (HUVEC) were seeded in 24 multiwell plates and cultured for 14 days in the presence of conditioned media from neuroblastoma cells that was changed every 2 days. The endothelial cells were fixed with 70% ethanol at room temperature for 30 minutes, incubated with anti-human anti-CD31 antibody (1:400) for 1h at 37^0 C, followed by incubation with goat anti-mouse conjugated to alkaline phosphatase. To visualize the vascular structures, cells were stained using 5-bromo-4-chloro-3-indolyl phosphate/nitro blue tetrazolium (BCIP/NBT) at room temperature until tubules develop a dark purple colour, washed with distilled H_2O and let to air dried. Images were captured using JuLI™ - Smart Fluorescent Cell Analyser and analysed using AngioSys 1.0 Image Analysis Software (Cellworks #ZHA-1800).

Constructs, transfection, retroviral/lentiviral infections. Human PML-I isoform and PML-IV isoform coding sequences were cloned into the pBabe puro and pBabe hygro retroviral vectors, respectively (9). shPML pLKO and pLKO scrambled lentiviral plasmids were a kind gift from the Everett's lab (32). pGIPZ eGFP PML, TSP2 and pGIPZ eGFP scrambled plasmids were purchased from Open Biosystems/Dharmacon and lentiviral supernatants were prepared according to the manufacturer's protocol (most efficient sequences were used for the study). The sequence of the shRNA (GIPZ Clone V3LHS_402844) used for TSP2 downregulation studies was TATATGTAAACGTCATTCT. After infection the cells were cultured in presence of puromycin or hygromycin to select for infected cells. For pGIPZ eGFP lentiviral infection, infected GFP+ cells with the highest level of plasmid expression were selected using FACS sorting. Overexpression and downregulation of PML protein was confirmed by Western blot and fluorescent immunostaining.

Antibodies. Rabbit anti-human pan PML (H238) (1:200 for Western blot and immunostaining, Santa Cruz, #SC-5621), mouse anti-human pan PML (PG-M3) (1:200 for immunostaining,

Santa Cruz, #SC-966), anti-mouse pan PML (1:100 for Western blot and immunostaining, Millipore, #05-718), rabbit anti-human PML-I (diluted 1/100; produced by Hugues De The), anti-NCAM (1:400, Chemicon, #AB5032), anti-HIF1α (1:1000, BD Biosciences, #6109059), anti-Sox10 (1:3000, produced in Michael Wegner's lab, a kind gift from Huiliang Li, UCL), anti-tyrosine hydroxylase (TH, 1:200, Millipore, #AB152), anti-p75 (1:250, Promega, #G3231), anti-actin (1:5000, Sigma, #A2172), anti-CD31 (1:50, BD Pharmingen, #550274; for mouse tissue), anti-CD31, mouse monoclonal (diluted 1/100; Dako Cytomation, Hamburg, Germany; for human tissue).

RNA extraction and quantitative real-time (qRT) PCR. Total RNA was extracted using RNAeasy Plus Mini Kit (Qiagen) and cDNA was synthesized using High Capacity RNA-to-cDNA Kit (Applied Biosystems) according to the manufacturer's instructions. qRT PCR was performed in Applied Biosystems 7500 Real-Time PCR System thermo cycler using Maxima™ SYBR Green qPCR Master Mix (Fermentas). PML mRNA was normalised by measuring β-actin mRNA levels. The following primers were used:

PML total sense 5'-GGTGCAGAGGATGAAGTGCT

PML total antisense 5'-AGGAAACCGTGCATGTCC

PML-I sense 5'-CTCAGGGTCCTGGACGAGAACC

PML-I anti-sense 5'-CACGGCCTTGGAGTAGATGC

β-actin sense 5'-CCAACCGCGAGAAGATGA

β-actin 5'-TCCATCACGATGCCAGTG

TSP2 sense 5'-CTTTAGCTGCTGCTTGTGCC

TSP2 antisense 5'-GCGTTAGATGCGCCTTTTCC.

In vivo experiments. Immunodeficient NOD/SCID female mice (purchased from Harlan; 10/group) were subcutaneously injected into both flanks with $1x10^6$ neuroblastoma cells. Tumour size was monitored with a calliper and calculated according to the formula: V=(length x width^2)/2. Transgenic human-MycN TH mice (strain 129/SvJ) were kindly provided by Dr. Louis Chesler (Institute of Cancer Research, London, UK). Wild type C57BL/6 mice were obtained from the Jackson laboratories (via Charles River Laboratories). All experimental procedures involving wild type and transgenic mice were approved by the University College London and were conducted under the Animal Scientific Procedures Act, 1986 (United Kingdom).

Microarray. Total RNA was extracted from IMR32 pBpuro and PML-I-OE using Qiagen RNeasy Mini Kit 74104 (n=2). cDNAs labelled were prepared with SuperScript III RT kit (Invitrogen) using 5 µl of total RNA. Microarray slides were pre-hybridized in 3X SSC, 0.1% (w/v) SDS and 10 mg/ml bovine serum albumin (BSA) at 60^0 C for 20 min. Following pre-hybridization, slides were washed with distilled water for 1 minute and isopropanol for 1 minute, dried with an airbrush and pre-scanned to check for any array defects.

The capture sequence-tagged cDNAs were hybridized onto the microarray slide for 16 h at 55^0 C in a SlideBooster SB400 (Advalytix) with the power setting at 27 and a pulse:pause ratio of 3:7. The slides were washed in 2xSSC, 0.2% (w/v) SDS for 10 min at 55^0 C and then for 10 min at room temperature. The slides were dried and hybridized with the Cy3 and Cy5 dendrimers (3DNA 900, Genisphere) following manufacturer's instructions. Dried slides were scanned using a Inno Scan 700 (Innopsys) using autocalibration to obtain optimized non-saturating images for each fluorophore and analysed using BlueFuse for Microarrays (BlueGnome).

The data underwent Cross Channel Correction, followed by Lowess Normalisation. After normalising the data, the mean fold ratio value was derived and a cyber-T test was performed to generate a p-value. The software BASE was used to carry out the normalization. The data has been deposited in NCBI's Gene Expression Omnibus (33) and is accessible through GEO Series accession number GSE78086 (https://www.ncbi.nlm.nih.gov/geo/query/acc.cgi?acc=GSE78086).

Pathway Analysis. Oligos with a p-value below 0.05 (Cyber *t*-test) and a fold ratio ≥1.5 for up-regulation or ≤0.67 for down-regulation were selected. This resulted in 1567 up-regulated and 1195 down-regulated oligos, of which 1219 and 876, respectively, could be uniquely mapped to Entrez gene IDs (Supplementary Table 1). We then tested both sets of genes for enrichment of known pathways from various databases provided by ConsensusPathDB (34). Pathways with q-value≤0.1 for ConsensusPathDB were considered significantly enriched (Supplementary Table 2).

Statistical analysis. Correlations were evaluated by the Spearman's rank correlation coefficient (rS); rS values from 0.40 to 0.59 were considered moderate, from 0.60 to 0.79 were considered strong, and from 0.80 to 1 were considered very strong; values below 0.4 were considered weak. To compare quantitative variables between two groups of observations, the non-parametric Mann-Whitney U test was used. Statistical significance of differences between experimental and control groups was determined by ANOVA with Tukey's multiple comparison

test using GraphPad Prism 3.0 software (GraphPad Software, Inc.). Survival curves were constructed by using the Kaplan-Meier method.

Results

We have previously shown that PML is expressed in neural progenitor/stem cells of the developing neocortex (9). In order to evaluate its expression during development of the peripheral nervous system, we performed immunohistochemical analysis of neural crest progenitors of the sympathetic nervous system and, postnatally, in the adrenal gland medulla. PML was found expressed in a subset of embryonic p75-positive progenitors delaminating from the neural tube and in TH-positive cells in the developing and adult adrenal medulla (Figure 1A). Similarly, *in vitro* cultures of neural tube-derived progenitors showed PML accumulating in a subset of p75- and Sox10-positive cells (Figure 1B).

As neuroblastoma is believed to originate from progenitor cells of the developing sympathetic nervous system (20), we evaluated PML expression in neuroblastomas arising in tyrosine-hydroxylase (TH)-MYCN-transgenic mice, and found that it was downregulated in most tumours analysed (Figure 1C). We next assessed the expression of PML in primary neuroblastoma patients at presentation by immunohistochemical or immunofluorescence analysis in two independent cohorts. We showed that PML expression is high in the adult human adrenal medulla, but it is generally low in neuroblastomas (Figure 1D; Supplementary Table 1, two separate cohorts). Notably, the cumulative survival probability of patients whose localised tumours contained more than 40% of PML positive cells was excellent, with 100% event free survival probability after 7 years from diagnosis (Figure 1E; Supplementary Table 1). In stark contrast, survival probability of patients whose tumours contained less than 40% PML positive cells was only 10% after 2 years (Figure 1E). There was a striking correlation between low expression (<40% positive cells) of PML and tumour recurrence in localised, low-risk, patients, suggesting that PML expression may represent an accurate biomarker of relapse (Supplementary Table 1). Using double-staining immunohistochemical analysis we also assessed a third and larger cohort (Supplementary Table 2) that included relapsed cases only for stage 3-4 tumours. It is important to note that in this cohort MYCN-amplified tumours displayed significantly higher PML expression than MYCN-non-amplified samples (Supplementary Table 2 and Supplementary Figure 1A). PML expression in MYCN-non-amplified tumours (all stages) and MYCN-non-amplified stage 4 tumours was significantly associated with a reduced risk of tumour relapse (Supplementary Table 2 and Supplementary Figure 1B, C).

We next investigated PML expression in a panel of neuroblastoma cell lines. As mentioned above, there are several splice variants that produce seven or more protein isoforms, which retain a common tripartite motif but vary in their C-termini (12, 35). Analysis of total PML expression by Western Blotting and immunofluorescence analyses using a pan-PML antibody showed that a number of cell lines display low PML expression, with the most prominent PML isoform migrating at around 90-100 kilodalton (kDa), which corresponds to the PML-I (and PML-II) isoforms (Figure 2A, B). The mRNA levels of PML-I generally correlate with the high-molecular weight PML isoform (Figure 2C). Interestingly, PML-I expression seemed to be associated especially with Schwannian or intermixed types (Figure 2A-C). These findings suggest that there is, at least in part, a selective expression of PML isoforms in neuroblastoma cell lines. We then assessed the effect of reconstituting PML expression in PML^{low} neuroblastoma cells. To this end, PML^{low} IMR32 cells were infected with retroviral vectors expressing PML-I or the tumour-suppressive PML-IV isoform (Figure 2D) and analysed for their growth properties. PML-IV-, but not PML-I-expressing cells showed a marginal but significant inhibition of proliferation compared to vector-infected control cells (Figure 2E). The PML-reconstituted cell lines were injected into the flanks of immunodeficient mice and tumour masses were measured at regular intervals for about 4 weeks. Experiments were terminated when the tumour size reached the upper limit allowed by UK and local animal welfare regulations. While neuroblastoma cells infected with the control or PML vectors formed tumours of comparable size, necroscopic and pathological analyses revealed that PML-I tumours were paler compared to control or PML-IV tumours (Figure 3A, B). Indeed, immunofluorescence analysis of the CD31 endothelial marker, revealed that there was a significant reduction in vascular clusters in PML-I compared to control tumours (Figure 3C). Furthermore, decreased angiogenesis in PML-I tumours correlated with enrichment in S100-positive Schwann-like cells, typically associated with low-risk forms of neuroblastoma (26, 27), and reduced number of cells expressing the neuroblast marker CD56 (Figure 3D). This effect did not appear related to a cell-autonomous effect of PML-I on S100, as expression of this marker was not increased in PML-I-overexpressing cells *in vitro* (not shown).

These results prompted us to investigate whether PML-I-expressing cells secrete antiangiogenic factor(s) that could explain the observed phenotype. We used supernatants from PML-I or empty vector-infected IMR32 cells in endothelial cell tubule formation assays with human umbilical vascular endothelial chord (HUVEC) cells. We observed inhibition of tubule number, length and branching when HUVEC cells were exposed to the PML-I, but not control, supernatants (Figure 3E). These *in vitro* results were corroborated by immunofluorescence

analysis in neuroblastoma patients that confirmed that there was a statistically significant inverse correlation between CD31 positive microvessel clusters and PML expression (Figure 3F, G and Table 1). Thus, PML regulates angiogenesis *in vitro* and *in vivo*.

We next studied the potential mechanisms involved. Based on previous studies (36), the PML-IV isoform controls angiogenesis via an mTOR/HIF1α/vascular endothelial growth factor (VEGF) axis in fibroblasts and prostate cancer. However, we failed to detect differences in HIF1α levels in either normoxic or hypoxic conditions (Supplementary Figure 2A), thus implicating different mechanisms underlying PML-I-mediated regulation of angiogenesis in neuroblastoma. Therefore, we set out to study the potential effect of PML-I on gene expression. We analysed gene expression in PML-I and pBabe control IMR32 cells using custom-made arrays. As expected, PML-I appears to modulate a number of genes involved in cell cycle control (see Pathway Analysis in Supplementary Table 3), but also some regulating angiogenesis (not VEGF). Among them, thrombospondin-2 [TSP2 (THBS2)], a known inhibitor of angiogenesis (37-39), displayed over 4-fold increased expression in PML-I-transduced cells (Supplementary Table 4). These findings were validated via quantitative PCR (QPCR) and Western Blotting (Figure 4A, B). A western blot confirming substantial overexpression of PML-I in neuroblastoma cells after retroviral infections is shown in Supplementary figure 2B. In order to define the involvement of TSP2 in PML-I-mediated suppression of angiogenesis, we transduced control or PML-I-expressing IMR32 cells with lentiviral vectors expressing TSP2-specific or control shRNAs (Figure 4C). Critically, while TSP2 knockdown in control cells did not affect angiogenesis, it rescued the suppressive phenotype caused by PML-I (Figure 4D). A western blot confirmed that the TSP2 shRNA did not change the levels of overexpressed PML-I in neuroblastoma cells (Supplementary Figure 2C). Finally, by using PML-I- and TSP-2-specific antibodies tissue sections from neuroblastoma patients were scored as the percentage of stained nuclear and cytoplasm respectively neuroblastoma cells (Figure 4E). We revealed a correlation between expression of PML-I and TSP-2 (Spearman's correlation rank r=0.89), suggesting that the functional relationship is conserved in primary neuroblastoma (Table 2). Overall, our findings indicate that the tumour suppressor PML suppresses angiogenesis at multiple levels via the specialised functions of two of its splice forms, PML-I and PML-IV.

Discussion

Localised tumours without amplification of MYCN is a group of particular interest due to a difficult risk estimation resulting in quite different therapeutic options (intermediate-risk

chemotherapy versus wait-and-see strategy without chemotherapy) (40, 41). In this study, we have established that loss of PML expression identifies patients with localised disease at risk of tumour relapse that will potentially benefit from chemotherapeutic treatment, suggesting that PML could be used as a marker to guide therapeutic intervention. Interestingly, PML did not appear to act as a growth suppressor in neuroblastoma, as transduction of the growth suppressive PML-IV isoform in PML^{low} neuroblastoma cells only marginally inhibited cell growth, whereas PML-I had no effect on either cell or tumour growth. In contrast, transduction of PML-I led to inhibition of angiogenesis both *in vitro* and *in vivo*. We cannot exclude that prolonged observation of tumour growth could have revealed differences in tumour size as well, but we could not extend the analysis due to animal welfare regulations. These data indicate an isoform-specific PML role in regulation of angiogenesis in neuroblastoma. Notably, PML expression inversely correlated with tumour angiogenesis index in patient samples. More generally, these findings suggest a novel role for tumour angiogenesis in relapse of localized tumours.

It is interesting to note that PML-IV was reported to inhibit angiogenesis via an mTOR/HIF1α-dependent mechanism (36), but we failed to detect an angiogenesis role of PML-IV in neuroblastoma nor changes in HIF1α protein levels. Instead, PML-I appears to work as a HIF1α–□□□□□□□□□□□ angiogenesis suppressor via transcriptional regulation of thrombospondin-2 (TSP2), a known inhibitor of angiogenesis and tumourigenesis (37, 38, 42). Although it remains to be determined how PML-I could regulate TSP2, our findings suggest that a novel PML-I/TSP2 signalling module suppresses tumour angiogenesis in neuroblastoma. Considering the effect of PML-I expression on the retinoblastoma pathway (see Pathway Analysis and (9)), one could speculate that pRb/E2Fs regulates *TSP2* gene expression. In this respect, as oncogenic RAS is known to inhibit the expression of TSP2 in tumour cells (43), it could be hypothesized that TSP2 induction could be part of a PML/pRb tumour suppressive checkpoint triggered by RAS activation in normal cells (44).

Another finding of our study is the association between reduced angiogenesis and increased expression of Schwann-like markers in PML-I-overexpressing tumours. The presence of Schwann-like differentiation in neuroblastoma is a good prognostic marker and has been found associated with reduced angiogenesis (45), although it is still debated whether cells carrying Schwann markers with neuroblastoma tumours are of tumour origin (46, 47). A previous report suggested that PML expression correlates with the Schwann-like phenotype in cell lines and that reintroduction of PML in PML^{low} Neuronal (N-type) cells induced neurite extension (48). However, we failed to observe a differentiation-promoting effect of PML in N-type IMR32 cells

nor increased expression of the Schwannian marker S100 *in vitro*. Thus, our study suggests that PML may regulate Schwannian differentiation within neuroblastoma tumours via angiogenesis inhibition or that TSP2 itself may have direct pro-differentiation properties *in vivo*. In keeping with this, TSP2 has been shown to induce synaptogenesis in the central nervous system (49) and chondrogenic differentiation in the bone (50).

In conclusion, our study reveals a novel PML-I/TSP2 axis regulating neuroblastoma angiogenesis and differentiation, which could serve as biomarker to predict relapse in localized neuroblastoma. More generally, PML is emerging as key player in angiogenesis regulation via the ability of two of its splice forms, PML-I (the present study) and PML-IV (36) to control different steps of the angiogenesis process.

Acknowledgments

This study was supported by a project grant from the Wellcome Trust to PS and AS. We thank the Pathology teams both at ICH (Dyanne Rampling) and Gaslini and the UCL Scientific Services, the Cancer Genome Engineering facility, the UCL Biological Services Unit and the Microarray Facility at Brunel University. PS leads the Samantha Dickson Brain Cancer Unit.

Funding

This work was in part funded by a Wellcome Trust project grant (to PS and AS). PS is funded by the Brain Tumor Charity among other funding bodies. AP and VP were supported by funds 'Cinque per mille' and 'Ricerca corrente' from the Italian Health Ministry to the Istituto Gaslini.

References

1. Sahin U, Lallemand-Breitenbach V, de The H. PML nuclear bodies: regulation, function and therapeutic perspectives. J Pathol. 2014;234(3):289-91.
2. Dellaire G, Bazett-Jones DP. PML nuclear bodies: dynamic sensors of DNA damage and cellular stress. Bioessays. 2004;26(9):963-77. Epub 2004/09/08.
3. Salomoni P, Pandolfi PP. The role of PML in tumor suppression. Cell. 2002;108(2):165-70.
4. Bernardi R, Pandolfi PP. Structure, dynamics and functions of promyelocytic leukaemia nuclear bodies. Nature reviews Molecular cell biology. 2007;8(12):1006-16. Epub 2007/10/12.
5. Salomoni P, Ferguson BJ, Wyllie AH, Rich T. New insights into the role of PML in tumour suppression. Cell Res. 2008;18(6):622-40.
6. Salomoni P. Stemming out of a new PML era? Cell Death Differ. 2009;16(8):1083-92. Epub 2009/06/13.
7. Koken MH, Linares-Cruz G, Quignon F, Viron A, Chelbi-Alix MK, Sobczak-Thepot J, et al. The PML growth-suppressor has an altered expression in human oncogenesis. Oncogene. 1995;10(7):1315-24.
8. Ablain J, de The H. Retinoic acid signaling in cancer: The parable of acute promyelocytic leukemia. Int J Cancer. 2014;135(10):2262-72.
9. Regad T, Bellodi C, Nicotera P, Salomoni P. The tumor suppressor Pml regulates cell fate in the developing neocortex. Nat Neurosci. 2009;12(2):132-40. Epub 2009/01/13.
10. Schreck KC, Gaiano N. PML: a tumor suppressor essential for neocortical development. Nat Neurosci. 2009;12(2):108-10.
11. Bischof O, Kirsh O, Pearson M, Itahana K, Pelicci PG, Dejean A. Deconstructing PML-induced premature senescence. Embo J. 2002;21(13):3358-69.
12. Condemine W, Takahashi Y, Zhu J, Puvion-Dutilleul F, Guegan S, Janin A, et al. Characterization of endogenous human promyelocytic leukemia isoforms. Cancer Res. 2006;66(12):6192-8.
13. Condemine W, Takahashi Y, Le Bras M, de The H. A nucleolar targeting signal in PML-I addresses PML to nucleolar caps in stressed or senescent cells. J Cell Sci. 2007;120(Pt 18):3219-27.
14. Rego EM, Wang ZG, Peruzzi D, He LZ, Cordon-Cardo C, Pandolfi PP. Role of promyelocytic leukemia (PML) protein in tumor suppression. J Exp Med. 2001;193(4):521-29.
15. Scaglioni PP, Yung TM, Cai LF, Erdjument-Bromage H, Kaufman AJ, Singh B, et al. A CK2-dependent mechanism for degradation of the PML tumor suppressor. Cell. 2006;126(2):269-83.

16. Trotman LC, Alimonti A, Scaglioni PP, Koutcher JA, Cordon-Cardo C, Pandolfi PP. Identification of a tumour suppressor network opposing nuclear Akt function. Nature. 2006;441(7092):523-7.
17. Ito K, Bernardi R, Morotti A, Matsuoka S, Saglio G, Ikeda Y, et al. PML targeting eradicates quiescent leukaemia-initiating cells. Nature. 2008.
18. Carracedo A, Weiss D, Leliaert AK, Bhasin M, de Boer VC, Laurent G, et al. A metabolic prosurvival role for PML in breast cancer. The Journal of clinical investigation. 2012;122(9):3088-100. Epub 2012/08/14.
19. Borriello A, Roberto R, Della Ragione F, Iolascon A. Proliferate and survive: cell division cycle and apoptosis in human neuroblastoma. Haematologica. 2002;87(2):196-214.
20. Brodeur GM. Neuroblastoma: biological insights into a clinical enigma. Nat Rev Cancer. 2003;3(3):203-16.
21. Altura RA, Maris JM, Li H, Boyett JM, Brodeur GM, Look AT. Novel regions of chromosomal loss in familial neuroblastoma by comparative genomic hybridization. Genes, chromosomes & cancer. 1997;19(3):176-84.
22. Maris JM, Matthay KK. Molecular biology of neuroblastoma. J Clin Oncol. 1999;17(7):2264-79.
23. George RE, Sanda T, Hanna M, Frohling S, Luther W, 2nd, Zhang J, et al. Activating mutations in ALK provide a therapeutic target in neuroblastoma. Nature. 2008;455(7215):975-8.
24. Mosse YP, Laudenslager M, Longo L, Cole KA, Wood A, Attiyeh EF, et al. Identification of ALK as a major familial neuroblastoma predisposition gene. Nature. 2008;455(7215):930-5.
25. Jiang M, Stanke J, Lahti JM. The connections between neural crest development and neuroblastoma. Current topics in developmental biology. 2011;94:77-127.
26. Shimada H, Ambros IM, Dehner LP, Hata J, Joshi VV, Roald B, et al. The International Neuroblastoma Pathology Classification (the Shimada system). Cancer. 1999;86(2):364-72.
27. Shimada H, Umehara S, Monobe Y, Hachitanda Y, Nakagawa A, Goto S, et al. International neuroblastoma pathology classification for prognostic evaluation of patients with peripheral neuroblastic tumors: a report from the Children's Cancer Group. Cancer. 2001;92(9):2451-61.
28. Matthay KK, Villablanca JG, Seeger RC, Stram DO, Harris RE, Ramsay NK, et al. Treatment of high-risk neuroblastoma with intensive chemotherapy, radiotherapy, autologous bone marrow transplantation, and 13-cis-retinoic acid. Children's Cancer Group. N Engl J Med. 1999;341(16):1165-73.
29. Brodeur GM, Pritchard J, Berthold F, Carlsen NL, Castel V, Castelberry RP, et al. Revisions of the international criteria for neuroblastoma diagnosis, staging, and response to treatment. J Clin Oncol. 1993;11(8):1466-77.
30. Ferreira-Facio CS, Milito C, Botafogo V, Fontana M, Thiago LS, Oliveira E, et al. Contribution of multiparameter flow cytometry immunophenotyping to the diagnostic screening and classification of pediatric cancer. PLoS One. 2013;8(3):e55534.
31. Pezzolo A, Parodi F, Marimpietri D, Raffaghello L, Cocco C, Pistorio A, et al. Oct-4+/Tenascin C+ neuroblastoma cells serve as progenitors of tumor-derived endothelial cells. Cell Res. 2011;21(10):1470-86.
32. Everett RD, Chelbi-Alix MK. PML and PML nuclear bodies: implications in antiviral defence. Biochimie. 2007;89(6-7):819-30. Epub 2007/03/09.
33. Edgar R, Domrachev M, Lash AE. Gene Expression Omnibus: NCBI gene expression and hybridization array data repository. Nucleic acids research. 2002;30(1):207-10. Epub 2001/12/26.
34. Kamburov A, Pentchev K, Galicka H, Wierling C, Lehrach H, Herwig R. ConsensusPathDB: toward a more complete picture of cell biology. Nucleic Acids Res. 2011;39(Database issue):D712-7.
35. Borden KL, Culjkovic B. Perspectives in PML: a unifying framework for PML function. Front Biosci (Landmark Ed). 2009;14:497-509.
36. Bernardi R, Guernah I, Jin D, Grisendi S, Alimonti A, Teruya-Feldstein J, et al. PML inhibits HIF-1alpha translation and neoangiogenesis through repression of mTOR. Nature. 2006;442(7104):779-85.
37. Tokunaga T, Nakamura M, Oshika Y, Abe Y, Ozeki Y, Fukushima Y, et al. Thrombospondin 2 expression is correlated with inhibition of angiogenesis and metastasis of colon cancer. Br J Cancer. 1999;79(2):354-9.
38. Volpert OV, Tolsma SS, Pellerin S, Feige JJ, Chen H, Mosher DF, et al. Inhibition of angiogenesis by thrombospondin-2. Biochem Biophys Res Commun. 1995;217(1):326-32.
39. Lawler PR, Lawler J. Molecular basis for the regulation of angiogenesis by thrombospondin-1 and -2. Cold Spring Harbor perspectives in medicine. 2012;2(5):a006627.
40. Oberthuer A, Hero B, Berthold F, Juraeva D, Faldum A, Kahlert Y, et al. Prognostic impact of gene expression-based classification for neuroblastoma. J Clin Oncol. 2010;28(21):3506-15.
41. Simon T, Spitz R, Hero B, Berthold F, Faldum A. Risk estimation in localized unresectable single copy MYCN neuroblastoma by the status of chromosomes 1p and 11q. Cancer Lett. 2006;237(2):215-22.

42. Hawighorst T, Velasco P, Streit M, Hong YK, Kyriakides TR, Brown LF, et al. Thrombospondin-2 plays a protective role in multistep carcinogenesis: a novel host anti-tumor defense mechanism. EMBO J. 2001;20(11):2631-40.
43. Pylayeva-Gupta Y, Grabocka E, Bar-Sagi D. RAS oncogenes: weaving a tumorigenic web. Nat Rev Cancer. 2011;11(11):761-74.
44. Ferbeyre G, de Stanchina E, Querido E, Baptiste N, Prives C, Lowe SW. PML is induced by oncogenic ras and promotes premature senescence. Genes Dev. 2000;14(16):2015-27.
45. Liu S, Tian Y, Chlenski A, Yang Q, Salwen HR, Cohn SL. 'Cross-talk' between Schwannian stroma and neuroblasts promotes neuroblastoma tumor differentiation and inhibits angiogenesis. Cancer Lett. 2005;228(1-2):125-31.
46. Ambros IM, Ambros PF. Schwann cells in neuroblastoma. European journal of cancer. 1995;31A(4):429-34.
47. Bourdeaut F, Ribeiro A, Paris R, Pierron G, Couturier J, Peuchmaur M, et al. In neuroblastic tumours, Schwann cells do not harbour the genetic alterations of neuroblasts but may nevertheless share the same clonal origin. Oncogene. 2008;27(21):3066-71.
48. Yu JH, Nakajima A, Nakajima H, Diller LR, Bloch KD, Bloch DB. Restoration of promyelocytic leukemia protein-nuclear bodies in neuroblastoma cells enhances retinoic acid responsiveness. Cancer Res. 2004;64(3):928-33.
49. Christopherson KS, Ullian EM, Stokes CC, Mullowney CE, Hell JW, Agah A, et al. Thrombospondins are astrocyte-secreted proteins that promote CNS synaptogenesis. Cell. 2005;120(3):421-33.
50. Jeong SY, Kim DH, Ha J, Jin HJ, Kwon SJ, Chang JW, et al. Thrombospondin-2 secreted by human umbilical cord blood-derived mesenchymal stem cells promotes chondrogenic differentiation. Stem Cells. 2013;31(10):2136-48.

Figure legends

Figure 1: PML expression is low in neuroblastoma compared with normal tissues and is a marker of high-risk tumours. (A) Immunofluorescence analysis of PML expression in sympathetic neurons during mouse development. PML is detectable in early neural crest p75+ progenitors in the neural tube, and in TH+ medullar cells in the developing and adult adrenal gland (scale bar 50□m); (**B**) Expression of p75, Sox10 and PML in neural crest progenitors *in vitro*. (**C**) PML expression is low in neuroblastomas arising in TH-MycN transgenic mice. Upper panel: Western blot analysis showing PML expression (indicated by the arrows) in tumours (T1-13) compared to normal adrenal gland (N). Equal loading was verified by blotting with an actin antibody (bottom gel). Lower panel; representative images of immunofluorescence analysis showing co-expression of PML and the neuroblast marker NCAM (numbers indicate tumours ID). (**D**) Immunohistochemical analysis demonstrating co-expression of PML in primary human neuroblastomas compared to normal adrenal gland. An anti N-CAM antibody was used to mark neuroblastic tumour cells (**E**) Low PML expression in localized human neuroblastomas is associated with increased probability of relapse ($p<0.0001$, Mann-Whitney test) and reduced cumulative survival probability ($p<0.0001$, log-rank test); immunofluorescence analysis of tumours from three patients is shown on the left.

Figure 2: Expression of PML isoforms in neuroblastoma cell lines and effect on cell growth. (**A**) Western blot analysis showing expression of total PML in neuroblastoma cell lines. Actin was used as loading control. Quantification of the western blot analysis is shown in the bottom. (**B**) Immunofluorescence analysis of total PML expression in neuroblastoma cell lines. (**C**) Reverse transcription Q-PCR analysis was used to assess the relative expression of total PML and the PML-I isoform in neuroblastoma cell lines. Primary glioblastoma neural stem cells (G4) and foetal neural stem cells (NSC) were used as negative and positive controls, respectively. The bars indicate the mean values from triplicate wells and the error bars standard errors. (**D**) Western blot analysis showing exogenous overexpression of the PML-I and IV isoforms in IMR32 cells. (**E**) Proliferation curves showing the growth rates of IMR32 cells transduced with an empty retroviral vector or viruses containing the PML-I and PML-IV isoforms, as indicated. Points in the curve are the mean values from triplicate wells and the error bars indicate standard errors.

Figure 3. PML-I inhibits angiogenesis in human neuroblastomas. (**A, B**) IMR32 cells expressing (PML-I-OE and PML-IV-OE) or non expressing (pBpuro and pBhygo) PML isoforms were injected into the flanks of immunodeficient mice. At the end of the experiment, tumours were excised and photographed (A panel). Tumour volumes were also measured every other day starting from one week after injections of neuroblastoma cells (B panel). Values represents means +/- SD, n=10 for PML-I/PML-IV and vector controls; stars refer to individual time points at which p-values were calculated, albeit not significant (t-test). **C**) CD31+ vascular clusters (indicated by the arrows) were detected in the xenotransplanted tumour using immunofluorescence analysis (left panels). Quantification of the experiment is shown in the right panel (*** = P<0.001). (**D**) Immunohistochemical analysis of representative sections of control (pBpuro) or PML-I overexpressing (PML-I-OE) tumour xenografts. The antibodies used are indicated (H&E=haematoxylin and eosin). (**E**) Angiogenesis assay. The upper panel shows images of the vascular structures in the presence of pro- (VEGF), anti- (Suramin) angiogenic factors or supernatants from cells expressing (PML-I OE) or non expressing (pBpuro) PML-I. Quantification of the experiment is shown in the bottom panel. Bars indicate the means of triplicate values and error bars the standard errors. (**F**) Microvessel clusters (red) in primary human neuroblastomas were detected by immunofluorescence analysis using a CD31 antibody; nuclei were counter stained with DAPI (blue). Scale bar = 32 μm. Representative image showing a tumour with high MCV/low PML (left) and a tumour with low MCV/high PML (right). (**G**) Graph showing a reverse correlation between the number of $CD31^+$ micro-vessel clusters and PML positive cells in the whole tumour area (Spearman's correlation rank r=-0.89).

Figure 4. PML-I induces expression of Thrombospondin 2 (TSP2), which is required for the antiangiogenic activity. (**A**) Reverse transcription Q-PCR analysis confirming overexpression of TSP2 in PML-I expressing cells (PML-I-OE) relative to control (pBpuro); the bars indicate the mean values of three independent experiments and error bars standard errors. (**B**) Western blot analysis showing increased expression of TSP2 protein in PML-I-expressing cells. Quantification of the western blot is shown in the right panel. (**C**) Western blot assay showing reduced expression of TSP2 in neuroblastoma cells transduced with a TSP2 shRNA with (PML-I-OE Sh) or without (pBpuro Sh) PML-I overexpression. It should be noted that PML-I overexpression (PML-I-OE) caused up regulation of TSP2 with respect to control cells (pBpuro). Quantification of the western blot is shown on the right. (**D**) Angiogenesis assay. The reduction in angiogenesis caused by incubation of HUVEC cells with supernatants from neuroblastoma cells overexpressing PML-I (PML-I-OE) was reverted by knockdown of TSP2 (PML-I-OE Sh).

Bars indicate the mean values of four independent experiments and error bars the standard errors. Representative images from the Angiogenesis assay are shown in the top of the panel. (**E**) Immunofluorescence analysis showing co-expression of PML-I and TSP2 in sections of primary human neuroblastomas. Statistical analysis shows a significant degree of correlation (Spearman's correlation rank r=0.89).

Table 1. Correlation of PML expression with tumor microvessel density in localised and metastatic tumors.

Table 2. Analysis of total PML, PML-I and TSP2 expression in localised and metastatic tumor

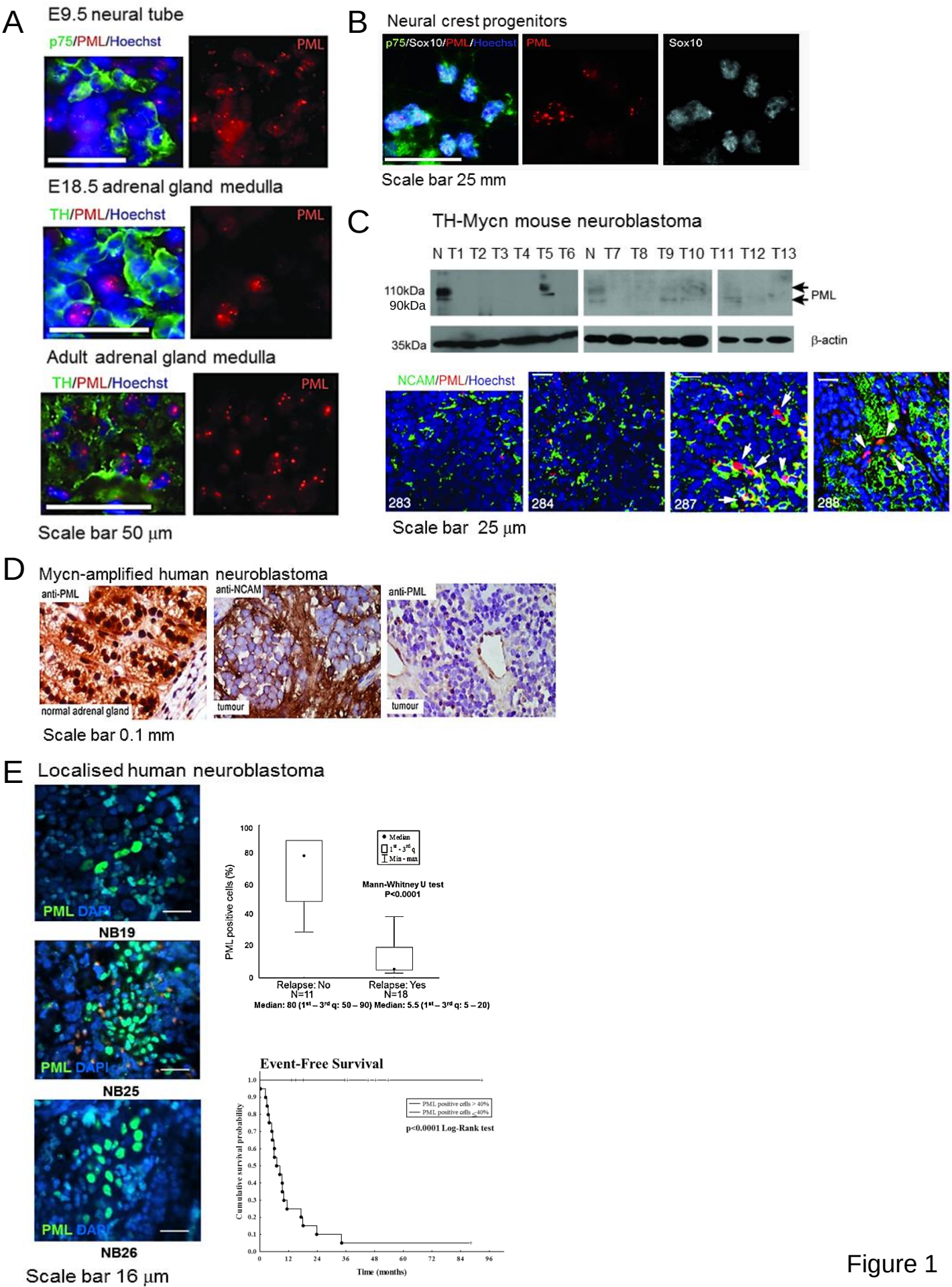
A
E9.5 neural tube
p75/PML/Hoechst
PML
E18.5 adrenal gland medulla
TH/PML/Hoechst
PML
Adult adrenal gland medulla
TH/PML/Hoechst
PML
Scale bar 50 μm
B
Neural crest progenitors
p75/Sox10/PML/Hoechst
PML
Sox10
Scale bar 25 mm
C
TH-Mycn mouse neuroblastoma
N T1 T2 T3 T4 T5 T6 N T7 T8 T9 T10 T11 T12 T13
110kDa
90kDa
PML
35kDa
β-actin
NCAM/PML/Hoechst
283
284
287
288
Scale bar 25 μm
D
Mycn-amplified human neuroblastoma
anti-PML
normal adrenal gland
anti-NCAM
tumour
anti-PML
tumour
Scale bar 0.1 mm
E
Localised human neuroblastoma
PML DAPI
NB19
PML DAPI
NB25
PML DAPI
NB26
Scale bar 16 μm
PML positive cells (%)
Median
1st - 3rd q
Min - max
Mann-Whitney U test
P<0.0001
Relapse: No
N=11
Relapse: Yes
N=18
Median: 80 (1st – 3rd q: 50 – 90) Median: 5.5 (1st – 3rd q: 5 – 20)
Event-Free Survival
PML positive cells > 40%
PML positive cells ≤ 40%
p<0.0001 Log-Rank test
Cumulative survival probability
Time (months)

Figure 1

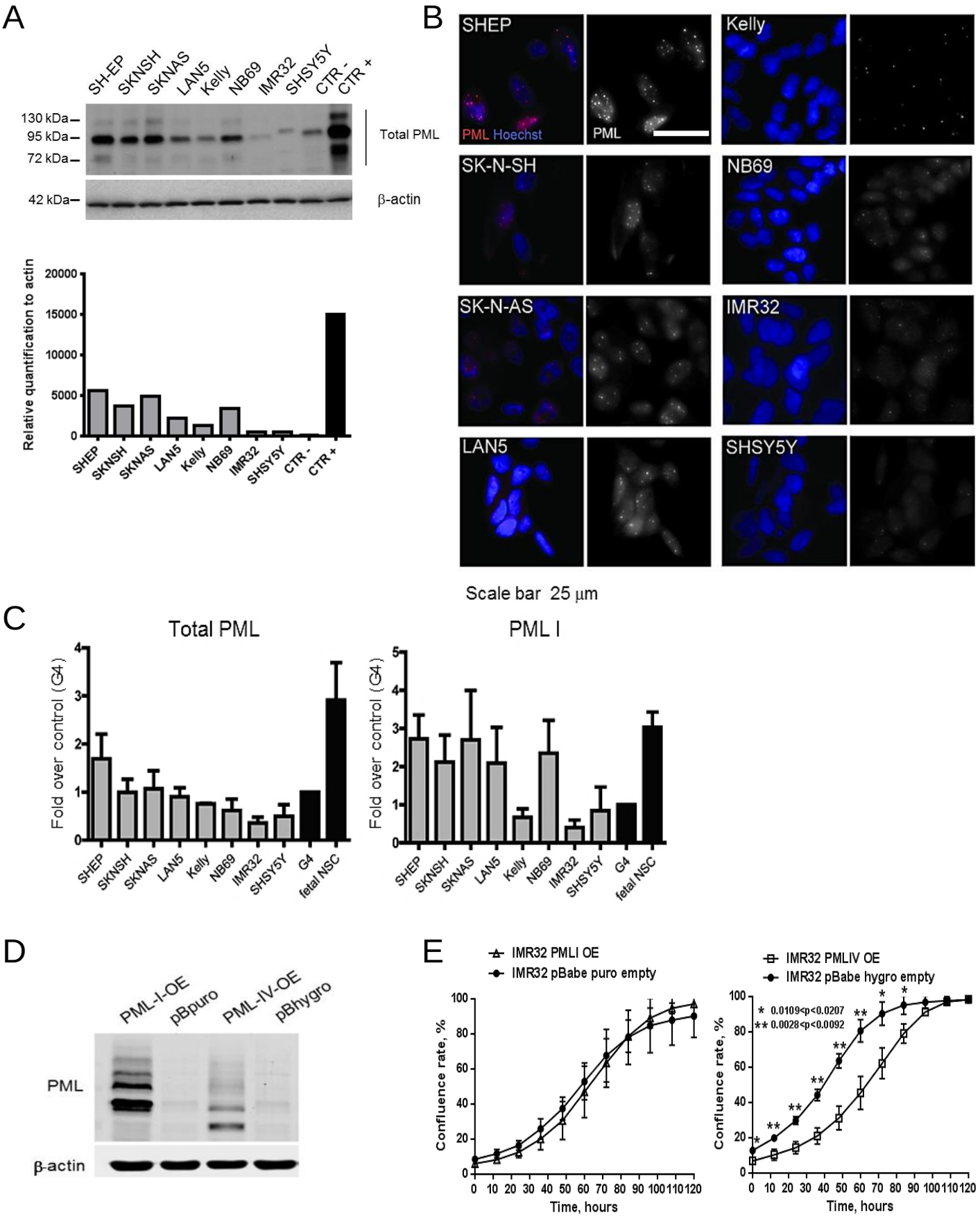
A
SH-EP
SKNSH
SKNAS
LAN5
Kelly
NB69
IMR32
SHSY5Y
CTR -
CTR +
130 kDa
95 kDa
72 kDa
Total PML
42 kDa
β-actin
Relative quantification to actin
20000
15000
10000
5000
0
SHEP
SKNSH
SKNAS
LAN5
Kelly
NB69
IMR32
SHSY5Y
CTR -
CTR +
B
SHEP
PML Hoechst
PML
Kelly
SK-N-SH
NB69
SK-N-AS
IMR32
LAN5
SHSY5Y
Scale bar 25 μm
C
Total PML
PML I
Fold over control (G4)
SHEP
SKNSH
SKNAS
LAN5
Kelly
NB69
IMR32
SHSY5Y
G4
fetal NSC
D
PML-I-OE
pBpuro
PML-IV-OE
pBhygro
PML
β-actin
E
IMR32 PMLI OE
IMR32 pBabe puro empty
IMR32 PMLIV OE
IMR32 pBabe hygro empty
Confluence rate, %
Time, hours
* 0.0109<p<0.0207
** 0.0028<p<0.0092

Figure 2

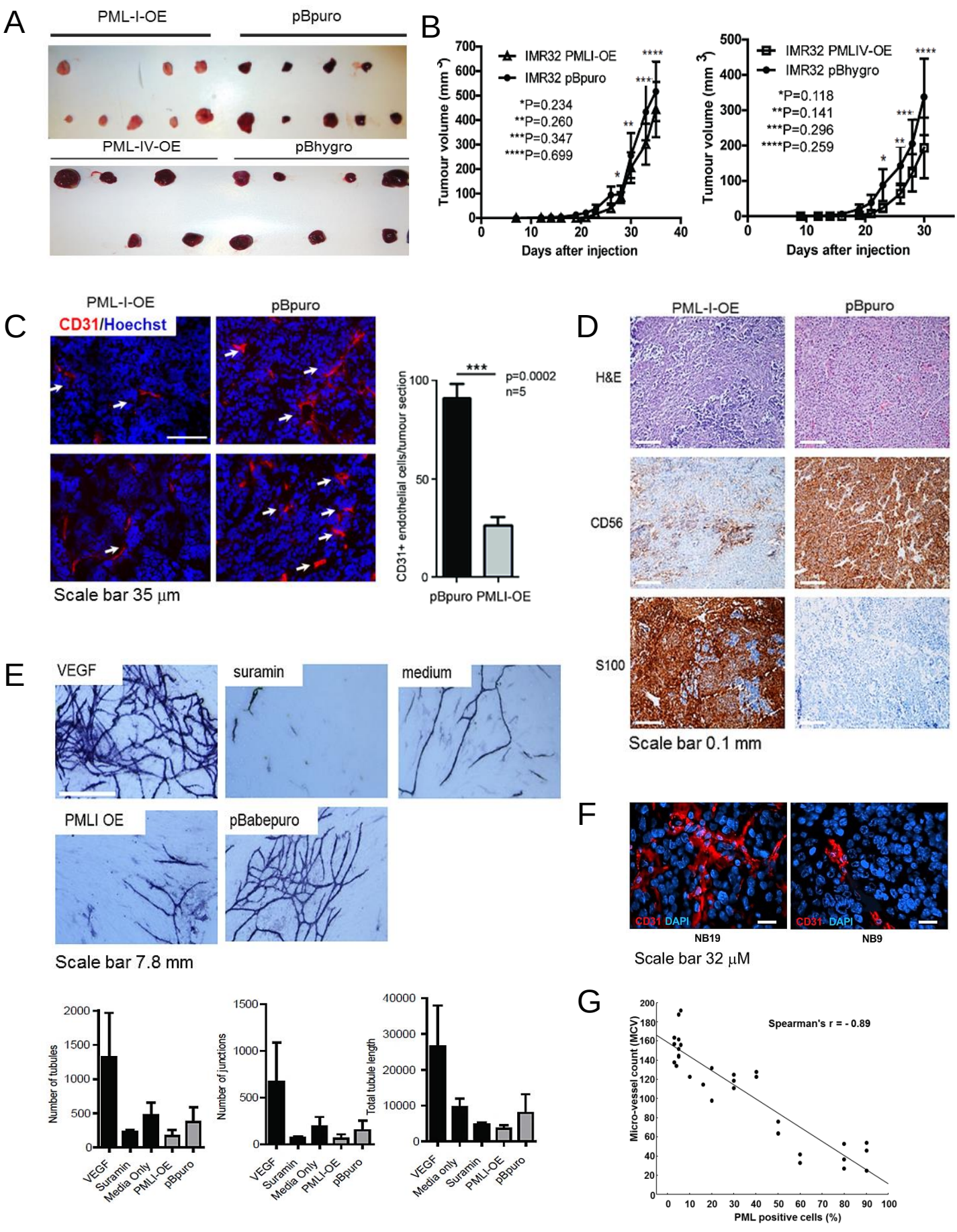
A
PML-I-OE
pBpuro
PML-IV-OE
pBhygro
B
IMR32 PMLI-OE
IMR32 pBpuro
*P=0.234
**P=0.260
***P=0.347
****P=0.699
Tumour volume (mm 3)
Days after injection
IMR32 PMLIV-OE
IMR32 pBhygro
*P=0.118
**P=0.141
***P=0.296
****P=0.259
C
PML-I-OE
pBpuro
CD31/Hoechst
Scale bar 35 μm
***
p=0.0002
n=5
CD31+ endothelial cells/tumour section
pBpuro PMLI-OE
D
PML-I-OE
pBpuro
H&E
CD56
S100
Scale bar 0.1 mm
E
VEGF
suramin
medium
PMLI OE
pBabepuro
Scale bar 7.8 mm
Number of tubules
Number of junctions
Total tubule length
VEGF
Suramin
Media Only
PMLI-OE
pBpuro
F
CD31 DAPI
NB19
NB9
Scale bar 32 μM
G
Spearman's r = - 0.89
Micro-vessel count (MCV)
PML positive cells (%)

Figure 3

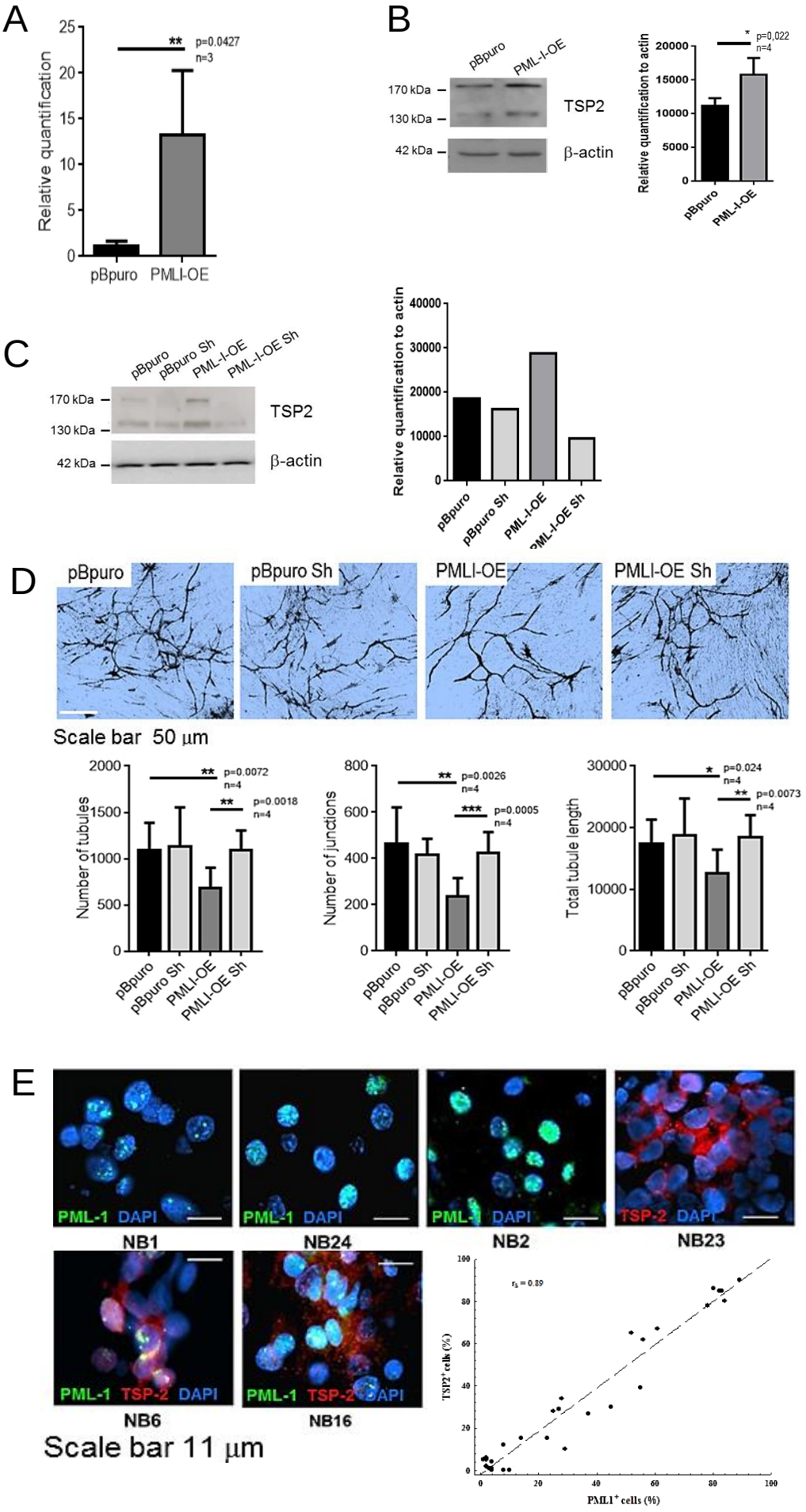
A
Relative quantification
**
p=0.0427
n=3
pBpuro
PMLI-OE
B
pBpuro
PML-I-OE
170 kDa
130 kDa
42 kDa
TSP2
β-actin
Relative quantification to actin
*
p=0.022
n=4
C
pBpuro
pBpuro Sh
PML-I-OE
PML-I-OE Sh
170 kDa
130 kDa
42 kDa
TSP2
β-actin
Relative quantification to actin
D
pBpuro
pBpuro Sh
PMLI-OE
PMLI-OE Sh
Scale bar 50 μm
Number of tubules
p=0.0072
p=0.0018
Number of junctions
p=0.0026
p=0.0005
Total tubule length
p=0.024
p=0.0073
E
PML-1 DAPI
TSP-2 DAPI
NB1
NB24
NB2
NB23
PML-1 TSP-2 DAPI
NB6
NB16
Scale bar 11 μm
TSP2+ cells (%)
PML1+ cells (%)

Figure 4

Table 1. Correlation of PML expression with tumor microvessel density in localised and metastatic tumors

Patient	Stage	MYCN ampl	Relapse	Outcome	PML+ cells (%)	MVC* (n)
NB1	1	N	N	CR	**90**	25
NB2	1	N	N	CR	**90**	46
NB3	1	N	N	CR	**80**	37
NB4	1	N	Y	CR	**20**	132
NB5	1	N	Y	CR	**3**	157
NB6	1	N	Y	CR	**40**	128
NB7	1	N	Y	CR	**6**	192
NB8	1	N	Y	CR	**5**	188
NB9	2A	N	N	CR	**80**	27
NB10	2A	N	N	AWED	**90**	54
NB11	2A	N	Y	CR	**20**	98
NB12	2A	N	Y	CR	**5**	145
NB13	2A	N	Y	CR	**4**	134
NB14	2A	N	Y	CR	**16**	115
NB15	2A	N	Y	CR	**40**	123
NB16	2B	N	N	CR	**80**	53
NB17	2B	N	Y	CR	**3**	164
NB18	2B	N	Y	DOD	**5**	152
NB19	2B	N	Y	DOD	**10**	123
NB20	2B	N	Y	AWED	**5**	144
NB21	4S	N	N	CR	**50**	64
NB22	4S	N	N	CR	**30**	119
NB23	4S	N	N	AWED	**50**	76
NB24	4S	N	N	CR	**60**	33
NB25	4S	N	N	AWED	**60**	42
NB26	4	Y	Y	DOD	**30**	111
NB27	4	Y	Y	DOD	**5**	162
NB28	4	Y	N	DOD	**30**	125
NB29	4	Y	Y	DOD	**3**	138
NB30	4	Y	Y	DOD	**6**	156

Abbreviations: N:no; Y:yes; AWED: alive with evidence of disease; DOD: dead of disease; CR: complete remission; MVC: micro-vessel count; n: number.

*Micro-vessels were visualized with anti CD-31 mab. The numbers of micro-vessels were calculated as the mean of the count in the tumor areas.

Table 2. Analysis of total PML, PML-I and TSP2 expression in localised and metastatic tumors

Patient	Stage	*MYCN* ampl	Relapse	Outcome	PML$^+$ cells (%)	PML-I$^+$ cells (%)	MVC* (n°)	TSP2$^+$ cells (%)
NB1	1	N	N	CR	90	82	25	85
NB2	1	N	N	CR	90	84	46	80
NB3	1	N	N	CR	80	80	37	86
NB4	1	N	Y	CR	20	29	132	10
NB5	1	N	Y	CR	3	10	157	0
NB6	1	N	Y	CR	40	37	128	27
NB7	1	N	Y	CR	6	4	192	1
NB8	1	N	Y	CR	5	2	188	6
NB9	2A	N	N	CR	80	83	27	85
NB10	2A	N	N	AWED	90	89	54	90
NB11	2A	N	Y	CR	20	23	98	15
NB12	2A	N	Y	CR	5	3	145	1
NB13	2A	N	Y	CR	4	1	134	5
NB14	2A	N	Y	CR	16	14	115	15
NB15	2A	N	Y	CR	40	45	123	30
NB16	2B	N	N	CR	80	78	53	78
NB17	2B	N	Y	CR	3	2	164	2
NB18	2B	N	Y	DOD	5	8	152	0
NB19	2B	N	Y	DOD	10	8	123	12
NB20	2B	N	Y	AWED	5	4	144	4
NB21	4S	N	N	CR	50	55	64	39
NB22	4S	N	N	CR	30	27	119	29
NB23	4S	N	N	AWED	50	52	76	65
NB24	4S	N	N	CR	60	61	33	67
NB25	4S	N	N	AWED	60	56	42	62
NB26	4	Y	Y	DOD	30	25	111	28
NB27	4	Y	Y	DOD	5	4	162	0
NB28	4	Y	N	DOD	30	28	125	34
NB29	4	Y	Y	DOD	3	2	138	5
NB30	4	Y	Y	DOD	6	2	156	2

Abbreviations: N:no; Y:yes; AWED: alive with evidence of disease; DOD: dead of disease; CR: complete remission; MVC: micro-vessel count; n: number.

MVC=Micro-vessels count. Micro-vessels were visualized with anti-CD31 mab. The numbers of micro-vessels were calculated as the mean of the count in the tumor areas.